

## PERFORMANCE OF THE CONDUCTION-COOLED LDX LEVITATION COIL

P. C. Michael<sup>1</sup>, J. H. Schultz<sup>1</sup>, B. A. Smith<sup>1</sup>, P. H. Titus<sup>1</sup>, A. Radovinsky<sup>1</sup>,  
A. Zhukovsky<sup>1</sup>, K. P. Hwang<sup>2</sup>, G. J. Naumovich<sup>3</sup>, and R. J. Camille, Jr.<sup>4</sup>

<sup>1</sup>MIT – Plasma Science and Fusion Center  
Cambridge, MA, 02139, USA

<sup>2</sup>Advanced Cryogenic Equipment, Inc.  
Emmaus, PA, 18049, USA

<sup>3</sup>Everson Tesla Incorporated  
Nazareth, PA, 18064, USA

<sup>4</sup>Myatt Consulting, Inc.  
Norfolk, MA, 02056, USA

### ABSTRACT

The Levitated Dipole Experiment (LDX) was developed to study plasma confinement in a dipole magnetic field. Plasma is confined in the magnetic field of a 680-kg Nb<sub>3</sub>Sn Floating Coil (F-coil) that is electromagnetically supported at the center of a 5-m diameter by 3-m tall vacuum chamber. The Levitation Coil (L-coil) is a 2800-turn, double pancake winding that supports the weight of the F-coil and controls its vertical position within the vacuum chamber. The use of high-temperature superconductor (HTS) Bi-2223 for the L-coil minimizes the electrical and cooling power needed for levitation. The L-coil winding pack and support plate are suspended within the L-coil cryostat and cooled by conduction to a single-stage cryocooler rated for 25-W heat load at approximately 20 K. The coil current leads consist of conduction-cooled copper running from room temperature to 80 K and a pair of commercially-available, 150-A HTS leads. An automatically filled liquid-nitrogen reservoir provides cooling for the coil's radiation shield and for the leads' 80-K heat stations. This paper discusses the L-coil system design and its observed cryogenic performance.

### INTRODUCTION

In the preliminary design of the Levitated Dipole Experiment (LDX), the Levitation Coil (L-coil) was a water-cooled, resistive electromagnet [1]. The chief drawback to a

resistive L-coil is that it requires a significant fraction of the deionized-water cooling capacity available to the experiment, cooling resources that could be better directed to other uses. Midway through the design of LDX, supplemental funding became available in the form of a Small Business Innovation Research (SBIR) grant for the design and construction of an HTS-based L-coil. The L-coil thus became the first HTS coil developed for use in a fusion-oriented, US plasma-physics experiment.

A key design feature that distinguishes LDX from previous levitated-dipole experiments is its emphasis on maximizing the magnetic-flux expansion around the Floating Coil (F-coil) [2]. To achieve the LDX physics goals, the L-coil must electromagnetically support the F-coil across an approximately 1.5-m gap, while imposing minimal distortion on the F-coil dipole field. An optimization code developed as part of the SBIR research was used to design the L-coil [3]. The optimal shape determined for the L-coil is that of a 2-cm tall, 1.3-m outer diameter, double-pancake winding.

## L-COIL AND CRYOSTAT DESIGN

### L-coil Description

The L-coil serves two functions within LDX. First, it electromagnetically supports the weight of the approximately 680-kg F-coil, and second, it is used in a position-control feedback loop to maintain the vertical position of the F-coil to within  $\pm 1$  mm of the center of the LDX vacuum chamber. Major features of the L-coil design are discussed in [4]. In brief, the L-coil is a 2800-turn, 0.41-m inner diameter, 1.32-m outer diameter, double-pancake winding that was wound using 7300 m of American Superconductor Corporation's (AMSC) Bi-2223 3-ply Narrow Wire. The transverse field component on the L-coil HTS, which is nearly constant across the coil's radial build, limits the operating current. At its designed operating current of 105 A, the L-coil produces an average transverse magnetic-flux density of 0.19 T on the HTS. By comparison, the peak axial flux density on the coil is 0.95 T. The anticipated critical current of the L-coil HTS at 20 K and 0.19 T transverse flux density is roughly 175 A, based on published AMSC scaling relations [5] and the average, 77-K, self-field, critical-current value of 63 A measured during quality assurance testing of the L-coil conductor.

The L-coil pancakes are wound to either side of a composite support plate. The support plate contains a 9.5-mm-thick stainless-steel core that helps to transfer the F-coil load to cryostat and two, 1.0-mm-thick OFHC copper sheets that are epoxy bonded to either side of the stainless-steel core to provide conduction cooling paths for the L-coil pancakes. Several radial cuts were machined into the copper sheets in an effort to limit eddy currents during ac operation. The thickness of the copper sheets was selected to provide less than 1-K temperature difference between the inner and outer diameters of the L-coil at its design heat load of 15 W [6]. The largest portion of the design heat load (approximately 12 W) was conservatively estimated using a full-penetration model for the magnetization hysteresis losses in the HTS that would result from the  $\pm 1$ -A, 1-Hz current ripple needed for F-coil position control [3].

A single layer of 125- $\mu$ m thick Nomex N196 was used as ground-plane insulation to maintain less than 1-K temperature difference between each pancake and the support-plate cooling sheets. Following vacuum impregnation of the coil, the top and bottom surfaces of the L-coil were covered with 3.2-mm-thick G-10 plates. 75- $\mu$ m-thick aluminum foil was epoxy bonded to the outward facing surface of these cover plates to reduce radiant heat transfer to the coil.

## Cryostat Description

FIGURE 1 shows a section view of the 1.45-m-diameter, 0.46-m-tall L-coil cryostat. The cryostat is cooled by the combination of a single-stage, Cryomech AL230 cryocooler (rated for 25 W heat load at approximately 20 K) and a liquid-nitrogen reservoir. Factory test data for our cryocooler shows a base temperature between 16.0 K and 16.4 K, and an average, low-end temperature rise of about 0.19 K for each 1 W of heat load. The trade-off between price, cooling capacity and minimum operating temperature, combined with ready access to liquid nitrogen in the LDX experimental hall, made this design a more attractive option than cooling by a large-capacity, multi-stage cryocooler.

The L-coil is suspended within the cryostat by a set of three, 3/8-16 threaded, stainless-steel rods. The support rods are attached to the L-coil by support arms whose ends are bolted at the inner and outer diameters of the support plate. To reduce thermal conduction to the coil, the mid-points of the support rods are thermally anchored through flexible copper straps to the bottom of the liquid-nitrogen reservoir. A thin layer of Apiezon N is used to improve thermal contact in all bolted thermal joints in the cryostat. The nitrogen reservoir is similarly suspended from the cryostat cover plate by a set of three stainless steel tubes, which also serve as nitrogen fill and vent tubes for the reservoir. The L-coil is completely surrounded by a copper radiation shield that is welded to the bottom of the nitrogen reservoir. The nitrogen reservoir and radiation shield are covered with 30 layers of NRC-2 super-insulation to reduce the radiation and convection heat loads from the room-temperature cryostat walls. The inner diameter of the approximately 140-kg radiation shield is supported from the cryostat cover plate by a set of three, 3/8-16 threaded, G-10 rods.

Lateral motion of the L-coil is restrained by a set of four, 0.5-m-long, 6-32 threaded, stainless-steel rods that extend from G-10 blocks on the support arms, through approximately 12-mm-diameter holes in the radiation shield, to mounting blocks on the outer shell of the cryostat. The rods are equipped at their room-temperature ends with spring-washer stacks. The number of washers in a stack can be reduced to provide stiffer support for shipping, or increased to reduce thermal-contraction loading during cool-down.

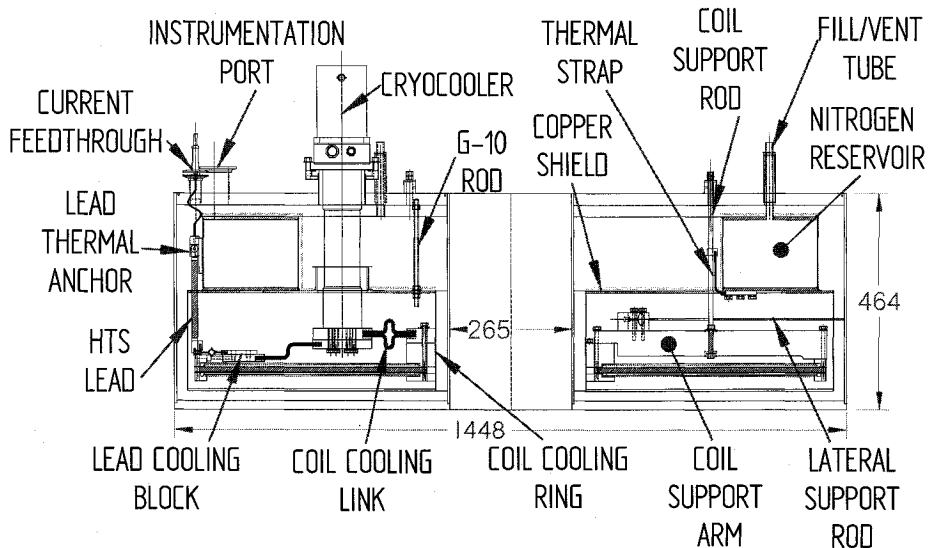


FIGURE 1. Section view of the L-coil cryostat.

## Coil Cooling Path

We installed forty, U-shaped copper clips to connect the upper and lower cooling sheets on the support plate. These clips are sandwiched to the support plate by a thick, copper cooling ring that is bolted through the support plate to a stainless-steel backing ring. The cooling ring is cut along a radius to reduce eddy currents during ac operation. The cut in the cooling ring is aligned with corresponding cuts in the support plate copper sheets. The cooling ring is connected by a fairly thick, laminated copper link to the cryocooler cold head. This cooling link is constructed from 250 layers of 50- $\mu\text{m}$ -thick, annealed OFHC copper sheet to minimize thermal-contraction loading of the cold head. The copper sheets were divided into two stacks during fabrication. A U-bend was pressed into the center of each stack and the stacks were combined with the U-bends facing outward. The ends of the stacks were then soldering together into end blocks using 60/40 lead-tin solder. One of these end blocks is indium soldered to the cryocooler cold head while the other is bolted to the L-coil cooling ring.

Due to an unfortunate incident during its vacuum impregnation, one of the pancakes developed a short to the support plate through the ground-plane insulation. Unfortunately, the short occurred at a location where it was inaccessible for repair. To restore the coil's electrical isolation, we decided to install a 38- $\mu\text{m}$ -thick sheet of Kapton MT in the interface between the cooling link and the coil cooling ring, and to isolate the coil support arms from their support rods using G-10 bushings and washers. The addition of an insulating sheet in the cooling link interface increased the thermal resistance between the cooling ring and cold head from our target value of less than 0.07 K/W [6] to about 0.14 K/W.

## Current Leads

The L-coil current leads consist of: conduction-cooled copper from room temperature to thermal anchors mounted on the outer wall of the nitrogen reservoir, and HTS leads from these reservoir thermal anchors to copper current jumpers at the coil terminals. The junctions between the copper and HTS parts of the leads consist of 24-mm-wide, 45-mm-tall, and 25-mm-thick OFHC copper blocks. For electrical isolation, the lead junction blocks are wrapped with a single, 25- $\mu\text{m}$ -thick layer of Kapton MT before they are clamped in the reservoir thermal anchors.

The copper portions of the leads consist of three, 1.5-mm-diameter copper wires. These wires are soldered together into commercially available 150-A vacuum feedthroughs at their upper ends and into the lead junction blocks at their lower ends. The copper portions of the leads are optimized for 125-A current [7], to provide some margin above the coil's 105-A operating point. The thermal anchors were each designed to accommodate a heat load of approximately 5.3 W (at 125 A) with less than 3.0 K temperature drop from the lead junction block to liquid nitrogen inside the reservoir.

The 230-mm-long, HTS portions of the leads were manufactured as Cryosaver® leads by AMSC to provide an operating current of up to 150 A at a maximum warm-end temperature of 80 K. The rated heat leak through the leads is 0.3 W/pair. The upper end of each HTS lead is indium soldered to a lead junction block while the lower end is connected through a 3-mm-thick, laminated copper strap and a 38- $\mu\text{m}$ -thick sheet of Kapton MT to an intermediate, lead cooling plate. This lead cooling plate in turn is connected through a 6.1-mm-thick, laminated copper strap to an end block that is mounted below and indium soldered to the cold head through the coil cooling link.

## Instrumentation

The L-coil and cryostat are instrumented for quench detection and to monitor thermal performance. The coil is equipped with a total of eight voltage taps. The voltage tap arrangement provides us with the ability to monitor voltage drops across: the copper portions of the current leads, the HTS portions of the current leads, both pancakes, and the entire L-coil.

The cryostat is equipped with a total of four MicroMeasurements Cryogenic Linear Temperature Sensors® (CLTS). The CLTS mounting locations include: one on the top plate of the radiation shield near a G-10 support rod, one on the bottom plate of the radiation shield near its average radius, one on the support rod end of its thermal strap, and one at the outer edge of the coil support plate. The cryostat is also equipped with a total of eight Lakeshore Cernox® temperature sensors. The Cernox mounting locations include: one each near the upper ends of the HTS leads, one each near the lower ends of the HTS leads, one on the cold head, one on the coil cooling ring, and one each on the surface, near the mean radius of each pancake. All of the sensor lead wires are taped, and bonded along a 0.15-m length to the outer shell of the nitrogen reservoir using Stycast type 2850® epoxy to provide a thermal anchor for the leads.

## INITIAL COOL-DOWN

The L-coil and cryostat were cooled together for the first time beginning in Apr. 2003. FIGURE 2 shows temperature vs. time traces for various cryostat components during this initial cool-down. FIGURE 2a shows temperature vs. time traces for components linked to the cryocooler, while FIGURE 2b shows traces for components linked to the liquid-nitrogen reservoir.

The cryocooler was activated first without adding any liquid nitrogen to the reservoir. After about 18 hr, when the coil temperature had reached approximately 200 K, we began a slow liquid-nitrogen transfer to the reservoir. We cooled the reservoir to liquid-nitrogen temperature over approximately 8 hr by controlling the nitrogen flow. After the nitrogen reservoir was full, the L-coil temperature continued to decrease to a base temperature of about 16.8 K, which was reached roughly 46 hr after the cool-down began. This cooling strategy was devised to limit the radial thermal displacements to about 1 mm between the lead thermal anchors on the nitrogen reservoir and the coil current terminals, and thus to minimize the bending loads on the HTS leads.

The temperatures at the cold head and at the lower ends of the HTS leads (FIG 2a) decreased rapidly during the first 5 to 6 hr of cool-down because of their relatively low thermal masses. The temperature difference between the cold head and the coil cooling ring peaked roughly 6 hr into cool-down at a maximum value of approximately 80 K, as the cold head began to slowly extract thermal energy out of the approximately 280-kg L-coil cold-mass. By contrast, the temperature difference between the coil cooling ring and the outer diameter of the coil support plate never exceeded 20 K; this relatively small temperature difference confirms that the support-plate cooling sheets maintain relatively uniform temperature across the pancakes even at very-high heat loads.

By the start of cool-down we could not evacuate the cryostat to below 1 mTorr even after a week of pumping, due to high outgassing of water vapor from the L-coil and the cryostat MLI. However, as the cryostat cooled, its vacuum pressure decreased steadily and settled to a value of about  $2 \times 10^{-7}$  Torr as the coil reached its 16.8-K base temperature.

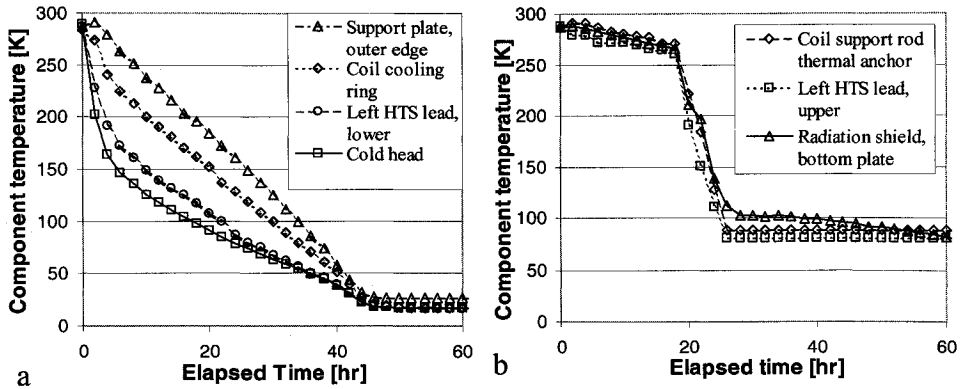


FIGURE 2. Temperature vs. time traces during the initial cool-down of the L-coil and cryostat. a) for components cooled by the cryocooler. b) for components cooled by the liquid nitrogen reservoir.

## AC EXCITATION

Two sets of small amplitude ac excitation experiments were performed on the L-coil. The first set was performed over the frequency range from 0.02 Hz to 5 Hz using a function generator and a  $\pm 20\text{-V}$ ,  $\pm 10\text{-A}$  bipolar operational-amplifier as the excitation source. Data from this set of measurements are relatively noise free and easy to interpret. The second set of experiments was performed over the same frequency range using  $\pm 1\text{-A}_{ac}$  ripple applied on top of a  $50\text{-A}_{dc}$  bias current. This set of experiments was performed using a 2-quadrant,  $\pm 100\text{-V}$ ,  $150\text{-A}$ , 12-pulse thyristor power supply, built specifically for the L-coil. The results from the second set of measurements are significantly noisier, but consistent with, those from the first set.

We processed the ac excitation data by splitting the measured coil voltages into two components, one that is in-phase with the excitation current and one that is  $90^\circ$  out-of-phase with the excitation current. The in-phase voltages were used to determine the effective coil inductance at each frequency while the out-of-phase voltages were used to determine the effective coil resistance. FIGURE 3 summarizes results from these experiments. FIGURE 3a shows the evaluated coil inductance vs. frequency, while FIGURE 3b shows the evaluated coil resistance vs. frequency. The open circles in these figures show results obtained with zero bias current, while the filled circles show results obtained with  $50\text{-A}_{dc}$  bias. The solid traces in these figures show simulated results from a model that features inductive coupling between the L-coil pancakes and their copper cooling sheets [8]; the fit between measurement and simulation is good.

The L-coil shows a significant drop in its effective inductance (FIG 3a) at frequencies above 0.5 Hz. This decrease is attributed to eddy-current circulation in the support-plate copper. At low frequencies, the resistive decay of the eddy currents occurs nearly as rapidly as the currents are induced, and so the eddy currents remain small. As the excitation frequency increases, the eddy currents are induced more rapidly than they decay and so the currents can increase to relatively large values. In the high frequency limit, the magnitude of the eddy currents is limited by the magnetic coupling between the L-coil and the cooling sheets. Because the magnetic flux generated by the cooling-sheet eddy currents effectively cancels that generated by the L-coil, the effective inductance for the L-coil decreases with frequency (FIG 3a). The eddy current losses show similar behavior. At low

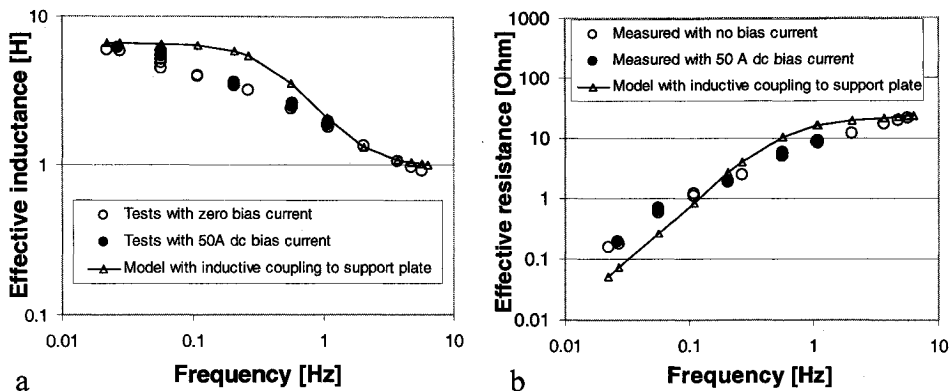


FIGURE 3. Results from the L-coil ac excitation experiments. a) Coil inductance vs. frequency. b) Effective coil resistance vs. frequency.

frequencies, the eddy losses are small because the eddy currents remain small, whereas at high frequencies, the eddy losses saturate as the eddy currents reach their limit value. Our eddy-current-coupling model indicates that roughly 90% to 95% of the total coil loss (FIG 3b) at frequencies above roughly 0.5 Hz is due to eddy-current loss in the coil cooling sheets [8].

We simulated the continuous operation of the L-coil in the LDX feedback-position-control loop by subjecting the coil to  $\pm 1$ -A, 1-Hz current ripple for a 1.5-hr time period. The coil's electrically-measured ac loss during the test was 4.3 W. By the end of the test, the temperature measured at the coil cooling ring had stabilized to a value 1.46 K above its initial value, while that measured at the cold head had risen by 0.86 K. The 0.60-K temperature drop from cooling ring to cold head is consistent with the value of 0.14 K/W for the thermal resistance through the insulated, coil cooling link. The 0.86-K temperature rise measured at the cold head indicates an ac heat load of approximately 4.5 W; the slightly higher heat load at the cold head is probably caused by additional eddy-current loss in the lead plate and coil cooling link.

## DC OPERATION

The L-coil was energized on its first attempt to its dc operating current of 105 A. FIGURE 4 summarizes temperature vs. operating-current data for various cryostat components during this test. FIGURE 4a shows temperatures measured near the upper ends of the HTS leads, while FIGURE 4b shows temperatures measured at the surface of the coil pancakes and at the coil cooling ring. We could not accurately determine the temperature from the cold-head temperature sensor due to a noisy signal during this experiment. The L-coil current was raised in a stepwise fashion and held constant for roughly 15 min following each step to check for voltage and temperature stabilization before proceeding to the next current step. As the L-coil current approached 105 A the size of the current steps was reduced to 1.5 A.

The temperatures near the tops of both HTS leads at zero current (FIG 4a) are about 81.4 K. Although these temperatures were already above the manufacturer recommended full-current operating temperature of 80 K, we decided to carefully proceed with the L-coil test anyway. The temperatures near the upper ends of these leads increase quadratically to

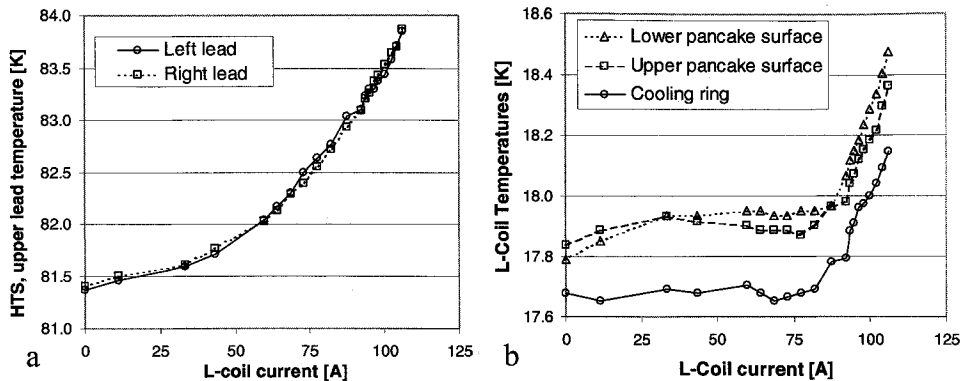


FIGURE 4. Temperature vs. current during first excitation of the L-coil to 105A. a) temperatures at upper ends of the HTS leads. b) temperatures at surface of L-coil pancakes and at the coil cooling ring.

values of about 83.8 K at 105 A current. The temperature measurements indicate that the thermal resistances from the lead junction blocks to the nitrogen reservoir are roughly 2.5 times larger than their design values. Although we cannot be certain, we presently believe that the higher than anticipated thermal resistances from the lead junction blocks result from insufficient clamping force to the reservoir thermal anchors.

The measured resistances for the HTS leads remained constant at currents up to 105 A. The left lead resistance was  $7.5 \mu\Omega$ , while the right lead resistance was  $9.3 \mu\Omega$ . The HTS lead resistances also include contributions from the copper current jumpers that attach the lower ends of the HTS leads to the coil terminals. The slightly higher resistance measured for the right lead occurs because the right lead's current jumper is about 2 cm longer in order to reach to the terminal on the lower pancake.

The measured coil temperatures (FIG 4b) do not change much as the coil current is increased from zero to approximately 75 A. Above 75 A, the coil temperatures increase steadily, with the cooling ring temperature rising from roughly 17.7 K at 75 A to roughly 18.2 K at 105 A. Because the L-coil power supply has a relatively large, high-frequency voltage ripple, the L-coil voltage could not be accurately measured. To estimate the coil performance, we reprocessed the cooling ring temperature vs. current data using heat-load factors derived from the ac excitation experiments to produce a heating power vs. current trace. FIGURE 5 shows the L-coil's estimated dc dissipation as its current is stepped from zero to 105 A. Also shown in this figure is the computed heating power vs. current for the L-coil conductor at an operating temperature of 20 K and index number of  $n=8$  [9]. The heating power vs. current trace in FIG 5 includes resistive dissipation in the L-coil's 55 joints and conductor splices, with an estimate, total resistance of  $11 \mu\Omega$ , as well as "index number" losses in the HTS. The correspondence between the two traces in FIGURE 5 is fairly good. The close similarity between the temperatures measured at the upper and lower pancakes (FIG 4b) suggests that they have roughly equivalent superconducting properties and that they are cooled more or less equally.

## HEAT LOADS

TABLE 1 summarizes the heat loads from various cryostat components to the liquid-nitrogen reservoir and to the cold head. The total, static heat load on the nitrogen reservoir

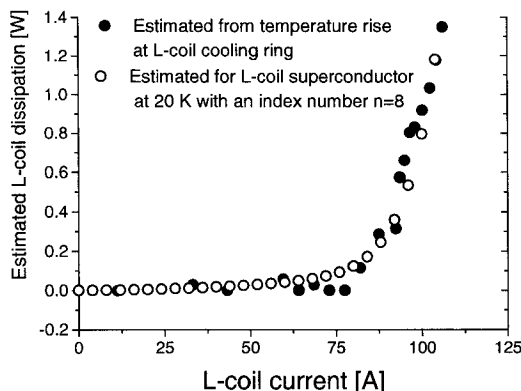


**FIGURE 5.** Estimated coil dissipation vs. current during initial operation of the L-coil to 105A.

is estimated at 24.9 W from its liquid-nitrogen boil-off rate of 0.56 l/hr. The static heat load on the cold head could not be precisely determined, but it is estimated at roughly 2.5 W from the 0.35-K temperature difference, measured at zero current, between the coil cooling ring and the cold head. The normalized, radiation and convection heat loads on the nitrogen reservoir and radiation shield are  $2.2 \text{ W/m}^2$ , which is just slightly larger than the design value of  $2.0 \text{ W/m}^2$ . All other heat loads on the nitrogen reservoir are within a few percent of their design values.

The measured ac heat load of 4.7 W at  $\pm 1\text{-A}$ , 1-Hz current excitation is significantly less than the 12-W value conservatively predicted by the full-penetration model used in the design code [3]. The bulk of this 4.7 W appears to result from eddy-current loss in the copper cooling sheets rather than hysteresis loss in the HTS [8]. The  $1.35\text{-W}_{\text{dc}}$  dissipation at 105-A current is significantly above our anticipated value of 0.29 W, calculated using the index number  $n=12$ , which was previously measured during our test of the L-coil in liquid nitrogen [4]. The apparent decrease in the L-coil's index number near 20 K is quite surprising, but may result from the radial temperature gradient across the L-coil which was present during the conduction cooled tests in the L-coil cryostat, but not during testing in the liquid nitrogen bath. This radial temperature gradient can produce a less uniform transition across the coil, resulting in a lower apparent index number.

**TABLE 1.** Heat loads on cryostat nitrogen reservoir and cold head.

Component	Heat load on nitrogen reservoir [W]	Heat load on cold head [W]
Nitrogen reservoir support tubes	3.75	-
Stainless steel coil support rods	2.85	0.39
G-10 support rods for radiation shield	0.15	-
Lateral support rods for the coil	-	0.16
Current leads (static)	5.75	0.3
Current leads at 105 A <sub>dc</sub>	9.10	0.3
Instrument lead wires	0.90	0.55
Radiation and convection heat loads	11.5	1.1
Coil dissipation at 105 A <sub>dc</sub>	-	1.35
AC loss with $\pm 1 \text{ A}$ , 1 Hz ripple at zero bias current	-	4.7
<b>Total at 105 A<sub>dc</sub> with <math>\pm 1 \text{ A}</math>, 1 Hz current ripple in L-coil</b>	<b>28.3</b>	<b>8.55</b>

## SUMMARY

A conduction-cooled, HTS L-coil was fabricated for use in LDX. The L-coil and cryostat were tested together for the first time during the time period from Apr. 2003 through June 2003 to evaluate the cryostat performance. The thermal performance of coil and cryostat were reasonably close to our design expectations. However, we did observe two significant deviations between measured and expected performance. First, the evaluated thermal resistances for the pressed thermal contacts between the lead junction blocks and the thermal anchors on the nitrogen reservoir were roughly 2.5 times larger than anticipated; the increased thermal resistance resulted in operating temperatures at the upper ends of the HTS leads significantly above their specified ratings. The design for the HTS portions of the leads appears to be significantly robust to permit us to stably operate the L-coil to its design current. Second, although the measured, total ac loss for the L-coil was less than its design value, the test results indicate significantly larger than anticipated eddy current loss in the support-plate cooling sheets at frequencies above 0.5 Hz. Because the ac loss in the L-coil HTS was very conservatively estimated during the coil design, we were able to absorb these eddy losses without severe consequences on the L-coil's thermal performance. The consequence of the support-plate eddy currents on the L-coil's magnetic performance in the LDX feedback position control loop remains to be determined.

## ACKNOWLEDGMENTS

The fabrication and test of the L-coil and L-coil cryostat were funded by the United States Department of Energy under the awards, DE-FC02-93ER54186, DE-FG02-98ER54458 and DE-FG02-98ER82529. We thank J. Stafiniak and C. Green of Everson Electric and R. Latons and C.Y. Gung of MIT-PSFC for their technical assistance during the assembly of the cryostat.

## REFERENCES

1. Schultz, J.H., Kesner, J., Minervini, J.V., Radovinsky, A., Pourrahimi, S., Smith, B., Thomas, P., Wang, P.W., Zhukovsky, A., Myatt, R.L., Kochan, S., Mauel, M. and Garnier, D., *IEEE Trans. Appl. Superconductivity* **9**, pp. 378-381 (1999).
2. Kesner, J., Bromberg, L., Garnier, D. and Mauel, M., *IAEA Fusion Engineering Conference 1998*, pp. 1165-1168 (1999).
3. Schultz, J.H., Driscoll, G., Garnier, D., Kesner, J., Mauel, M., Minervini, J.V., Smith, B., Radovinsky, A., Snitchler, G. and Zhukovsky, A., *IEEE Trans. Appl. Superconductivity*, **11**, pp. 2004-2009 (2001).
4. Michael, P.C., Zhukovsky, A., Smith, B.A., Schultz, J.H., Radovinsky, A., Minervini, J.V., Hwang, P. and Naumovich, G.J., *IEEE Trans. Appl. Superconductivity*, **13**, pp. 1620 – 1623 (2003).
5. American Superconductor Corporation, "Bi-2223 High Current Density Wire FactSheet," Westborough, MA, Oct. 1999.
6. Radovinsky, A., MIT-Plasma Science and Fusion Center, LDX project memo LDX-MIT-ALRadovinsky-010501-1, Jan. 5, 2001.
7. McFee, R., *Rev. Sci. Instr.* **20**, pp. 98-102 (1959).
8. Michael, P.C., MIT-Plasma Science and Fusion Center, LDX project memo LDX-MIT-PMichael-090503-1, Sept. 5, 2003.
9. Michael, P.C., MIT-Plasma Science and Fusion Center, LDX project memo LDX-MIT-PMichael-062703-1, June 27, 2003.